The Astrophysical Journal Supplement Series, 169:21–27, 2007 March

*z*BOOTES: *z*-BAND PHOTOMETRY IN THE NOAO DEEP WIDE-FIELD SURVEY BOOTES FIELD

Richard J. Cool[1]

Received 2006 October 17; accepted 2006 November 1

ABSTRACT

We present *z*Bootes, a new *z*-band photometric imaging campaign of 7.62 deg^2 in the NOAO Deep Wide-Field Survey (NDWFS) Bootes field. In this paper, all of the images for this survey are released as well as the associated catalogs. The final *z*Bootes catalogs are complete (at the 50% level) to 22.7 mag over 50% of the field. With these depths, the *z*Bootes images should be sensitive to L^* galaxies to $z \sim 1$ over much of the survey area. These data have several possible applications including searching for and characterizing high-redshift quasars and brown dwarfs and providing added constraints to photometric redshift determinations of galaxies and active galaxies to moderate redshift. The *z*Bootes imaging adds photometric data at a new wavelength to the existing wealth of multiwavelength observations of the NDWFS Bootes field.

Subject headings: astronomical data bases: miscellaneous — catalogs — galaxies: photometry — surveys

1. INTRODUCTION

In recent years, a number of multiwavelength surveys have been completed in order to understand the evolution of the multiwavelength properties of galaxies and active galactic nuclei (AGNs) throughout cosmic history. Deep observations spanning from the ultraviolet to the radio are time consuming, and obtaining spectroscopic follow-up observations of cataloged galaxies and AGNs requires many nights on the largest telescopes available. Thus, the area covered by many of the deepest multiwavelength surveys is fairly small. With the advent of new wide-field optical and near-infrared imagers and multiobject spectrographs, as well as superb new space facilities such as *GALEX* and *Spitzer*, the amount of the sky observed at all possible wavelengths is growing steadily.

One of the early deep, wide area, optical surveys, the NOAO Deep Wide-Field Survey[2] (NDWFS; B. T. Jannuzi et al. 2007, in preparation; A. Dey et al. 2007, in preparation) consists of two $\sim$9 deg^2 fields (the Bootes and Cetus fields) with excellent optical (B_W, R, and I) and near-infrared (K_s) photometry. The NDWFS Bootes field has become a popular target for many investigators and now has been observed across the full electromagnetic spectrum. Deep *GALEX* pointings provide near and far-ultraviolet photometry for the field; the NDWFS images consist of optical and near-infrared coverage, and the FLAMINGOS Extragalactic Survey (FLAMEX; Elston et al. 2005) observed the field to deep limits in J and K_s. *Spitzer* has imaged the Bootes field with both the Infrared Array Camera (Eisenhardt et al. 2004; *Spitzer* Shallow Survey) and the Multiband Imaging Photometer for *Spitzer*. Radio observations include deep Westerbork observations at 1.4 GHz (de Vries et al. 2002) and imaging by the Faint Images of the Radio Sky at Twenty-Centimeters survey (FIRST; Becker et al. 1995). *Chandra* has observed the Bootes field for 5 ks (XBootes; Murray et al. 2005; Kenter et al. 2005). Optical spectroscopy for several highly complete samples of galaxies and AGN has been completed with the Hectospec multiobject spectrograph on the MMT as part of the AGN and Galaxy Evolution Survey (AGES; C. Kochanek 2007, in preparation). A small region in the Bootes field was observed as part of the Large Area Lyman-Alpha survey to search for galaxies at very high redshifts (Rhoads et al. 2000). These data sets have allowed searches for high-redshift quasars and low-mass stars using mid-infrared selection techniques (Stern et al. 2006), studies of the quasar luminosity function (Brown et al. 2006; Cool et al. 2006), the clustering of high-redshift galaxies (Brown et al. 2003, 2005; Stanford et al. 2005; Rhoads et al. 2004), Lyα-emitting galaxies (Wang et al. 2004; Dey et al. 2005; Dawson et al. 2004; Rhoads et al. 2003), the broadband properties of AGNs (Brand et al. 2005, 2006b; Stern et al. 2006, 2005), the X-ray properties of AGNs (Brand et al. 2006a; Kollmeier et al. 2006), the spectral properties of infrared sources (Weedman et al. 2006; Desai et al. 2006; Khan et al. 2005; Higdon et al. 2005), and many other topics.

In this paper, we present new *z*-band observations of 7.6 deg^2 in the NDWFS Bootes region. These catalogs reach several magnitudes deeper than the public imaging released by the Sloan Digital Sky Survey (SDSS) and will provide a useful intermediate photometric measurement between the *I*-band data from NDWFS and near-infrared photometry from FLAMEX. We release the catalogs and reduced images for public use. Throughout this paper, all magnitudes are AB magnitudes (Oke 1974).

2. OBSERVATIONS

The *z*Bootes imaging survey was completed with the 90Prime wide-field imager (Williams et al. 2004) at prime focus on the Bok 2.3 m Telescope located on Kitt Peak. This instrument consists of four 4096 × 4096 thinned CCDs, providing excellent quantum efficiency in the blue, read out using eight amplifiers. The chips are arranged in a windowpane pattern with 10′ gaps between each of the CCDs. Each CCD images a 30'x30′ field on the sky with 0.45″ pixels. The southeast CCD has a large electron trap, making 13% of the area on that chip unusable for photometric measurements. These pixels are masked throughout the reduction process and are excluded when images are stacked.

The data were obtained between 2005 February 28 and 2005 March 31. Sky conditions varied from photometric to moderate levels of cirrus throughout the observations. The typical seeing during these observations was 1.6″. In total, we completed observations for eight 90Prime pointings within the NDWFS Bootes region. At each location, we obtained several dithered 300 s exposures (typically 12 exposures per field). The telescope was moved $\sim$1′ for each dither. The total number of exposures for each field was determined by the conditions at the time of the

[1] Steward Observatory, Tucson, AZ; rcool@as.arizona.edu.
[2] See http://www.archive.noao.edu/ndwfs http://www.noao.edu/noao/noaodeep.

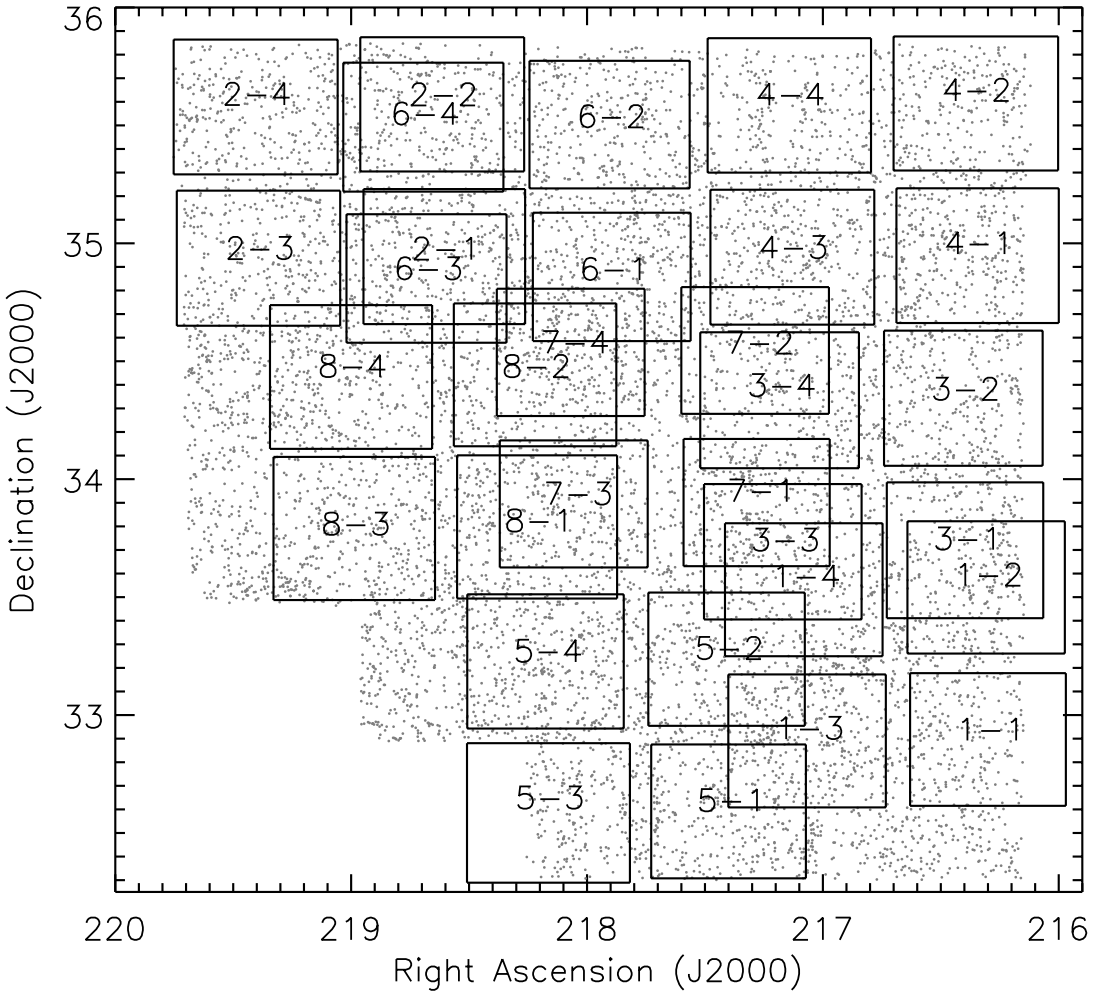

FIG. 1.—Map of the NDWFS survey area with the coverage of the *z*Bootes catalog overlaid. The gray points illustrate the distribution of 25% of the $I < 21.5$ galaxies in the NDWFS catalogs. Each of the subfields of the *z*Bootes imaging is labeled with the field number. The *z*Bootes imaging covers 7.6 deg^2 centered on the NDWFS Bootes Field, providing another set of data to the current suite of multiwavelength observations completed in this region.

observations. All of the exposures for a single field were obtained on the same night. As the gaps between CCDs on 90Prime are rather large, we did not attempt to make our dither pattern large enough the fill the regions between each CCD. This strategy avoids having nonuniform depth across a single field but results in gaps in our photometric coverage of the NDWFS survey field. Figure 1 shows the region covered in the *z*Bootes survey compared to the NDWFS Bootes Survey area. Throughout the rest of this paper, each of the fields imaged by a single 90Prime CCD is treated independently.

3. REDUCTIONS

All of the raw *z*Bootes images were processed using a combination of home-grown IDL routines and various tasks available within the Image Reduction and Analysis Facility (IRAF). Each image was bias and overscan corrected and known bad columns are removed by interpolating neighboring columns. On each night of clear skies, observations of the twilight sky were taken to generate a flat-field image that was divided into each object frame to correct for pixel-to-pixel variations in the CCD sensitivity.

While the thinned-chip nature of the CCDs on 90Prime allows for high efficiency in the blue, it also results in strong fringing in the reddest bands where the night sky spectrum is dominated by a forest of emission lines. On each night of observation, between 12 and 42 individual dithered images were obtained for this project in the z band. To generate a master fringe frame, we first removed any large-scale gradient in the background of each input image. The strength of the fringe pattern was then measured on each image and a multiplicative scale factor was applied to correct for any differences from the mean. We generated a master fringe frame by taking the median of all of the individual images taken on a single night of observations. This fringe frame was scaled to match the average strength of the fringes in each individual exposure and subtracted. This process was iterated (typically twice) until the fringe pattern was no longer present in each individual exposure. The left and middle panels of Figure 2 show a region of a single exposure before any processing and after the fringe pattern was been removed.

The astrometry of each image was calibrated by locating stars with $17 < z < 19$ from the Sloan Digital Sky Survey (SDSS) DR4 (Adelman-McCarthy et al. 2006). We fitted the astrometric solution with a fifth-order TNX world-coordinate system (WCS) using the IRAF task CCMAP. The images were then deprojected onto a rectilinear pixel system using the task MSCIMAGE in the MSCRED package in IRAF. Finally, aperture photometry of several stars in the magnitude range $17 < z < 19$ was performed on each of the input frames in order to determine offsets in the background level and photometric zero point between each of the frames. Any variations in the mean background or transparency were corrected before the individual images were stacked to create

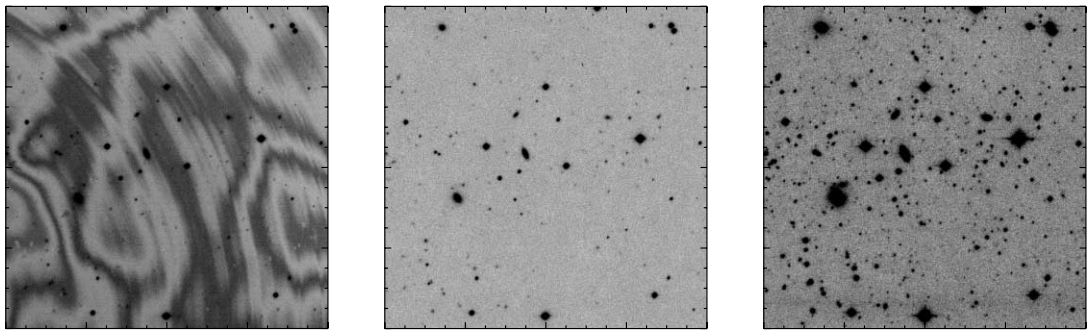

FIG. 2.—Example of the reduction steps performed on the zBootes imaging data. Left panel shows a portion of a raw data frame taken with 90Prime. Middle panel illustrates the same frame after flat-fielding and fringe correction. The final co-added frame, including all of the observations for this field, is shown in the right panel. Each of the images is 800 pixels on a side corresponding to $\sim 6'$. The total exposure time for this field was 1 hr.

the final co-added frame for each field. Pixels with values more than 3 σ from the mean were clipped when creating the final mosaic; this clipping rejected any cosmic rays present in the individual frames. Figure 2 shows a portion of a final stacked image.

The photometric zero point for each stacked image was determined by comparison with photometry publicly available from the SDSS (Adelman-McCarthy et al. 2006). Aperture photometry for stars with $18 < z < 19$ was compared to SDSS PSF magnitudes. The mean magnitude offset between the two photometric measurements was adopted as the magnitude zero point of the field. In general, the dispersion around this median was on the order of $\sigma_z \sim 0.03$ mag, comparable to the photometric scatter expected due to errors in the SDSS photometry (Ivezić et al. 2004). As the effective response of the z-band filter used in our work (including the effects of mirror reflectance and sky absorption) is likely different from that of the SDSS system, we examined the residuals between the zBootes photometry and the SDSS photometry as a function of the SDSS $i - z$ color of each object. The photometric residuals showed no correlation with the object color, and thus no color term has been applied to the zBootes photometry.

Several of the zBootes fields overlapped significantly. These regions of significant overlap were co-added, weighted by seeing and signal-to-noise in each input frame, to create mosaicked images of the overlap regions. Before co-adding the individual images in the overlap regions, each of the input images were background-subtracted, and the measured counts per pixel were converted to a true flux density per pixel measurement using the photometric zero point determined from comparison with public SDSS photometry discussed above. Figure 3 illustrates the area of the zBootes field included in these co-added observations compared to the object distribution in the NDWFS optical catalogs.

4. SOURCE CATALOGS

4.1. *Catalog Generation*

We constructed catalogs for each zBootes field using Source Extractor (SExtractor) version 2.3 (Bertin & Arnouts 1996). We detected objects using a 0.9″ FWHM Gaussian convolution kernel and enforced a 3 σ detection threshold. Pixels were weighted according to the number of input exposures that contributed to each in order to prevent the detections of a large number of spurious sources around the edges of each field that have fewer average observations and thus higher background noise than the centers. For each object detected in the catalog, we measured the flux in $\sim$100 apertures (with diameter 3″, 5″, and 7″) in a 6′ radius around the object. We used the interval containing 68.7% of the measurements as a measurement of the photometric error for each object. The simulated photometric errors we calculate from this method are about a factor of 2 larger than those measured by SExtractor.

Catalogs were also constructed for each of the stacked images created for the overlapping zBootes fields using the same process as used for individual subfields. The final zBootes catalog was constructed by checking each object for duplicate observations. For any object that was observed multiply, we define the best observation to be the measurement with the smallest simulated photometric errors. The final zBootes catalogs consist of over 200,000 objects.

Objects in the final zBootes catalogs were matched to detections in the NDWFS catalogs (DR3). For each NDWFS subfield, we checked for systematic offsets in both right ascension and declination between the zBootes astrometric system and the NDWFS reference frame. After removing any net offset between the NDWFS catalogs and our zBootes catalogs (which are discussed in more detail in § 4.3), the two object lists were matched with a 1″ match tolerance and the name and coordinates of the closest match NDWFS detection were recorded in the final zBootes catalog.

4.2. *Photometric Accuracy*

The final residuals between zBootes and SDSS photometric measurements for well-detected stars whose photometry is not affected by nonlinearity in the 90Prime CCDS are centered around zero with a 1 σ dispersion of 0.035 mag. The average quoted photometric error for the SDSS stars is 0.03 mag, and thus the majority of the final calibration error in the zBootes catalog can be attributed to photometric scatter in the SDSS photometry. The remainder of the scatter in the photometric calibration is likely due to errors in the large-scale flat-field corrections to each frame and imperfect subtraction of the strong fringing the 90Prime CCDs.

Since 1.25 deg^2 were observed more than once in the zBootes imaging, we can quantitatively estimate the error in our photometric measurements, both from calibration errors and reduction imperfections. The distribution of fluxes for the $\sim$7200 stars with $17 < z < 20$ observed two or more times within zBootes itself has zero mean and a 1 σ dispersion of 0.03 mag, in good agreement with the scatter in photometric calibration estimated above.

4.3. *Astrometric Precision*

As the zBootes astrometry was calibrated to the SDSS reference system, the agreement between SDSS and zBootes astrometry is quite good. Figure 4 shows the differences between SDSS, zBootes, and NDWFS astrometry. The dispersion between the

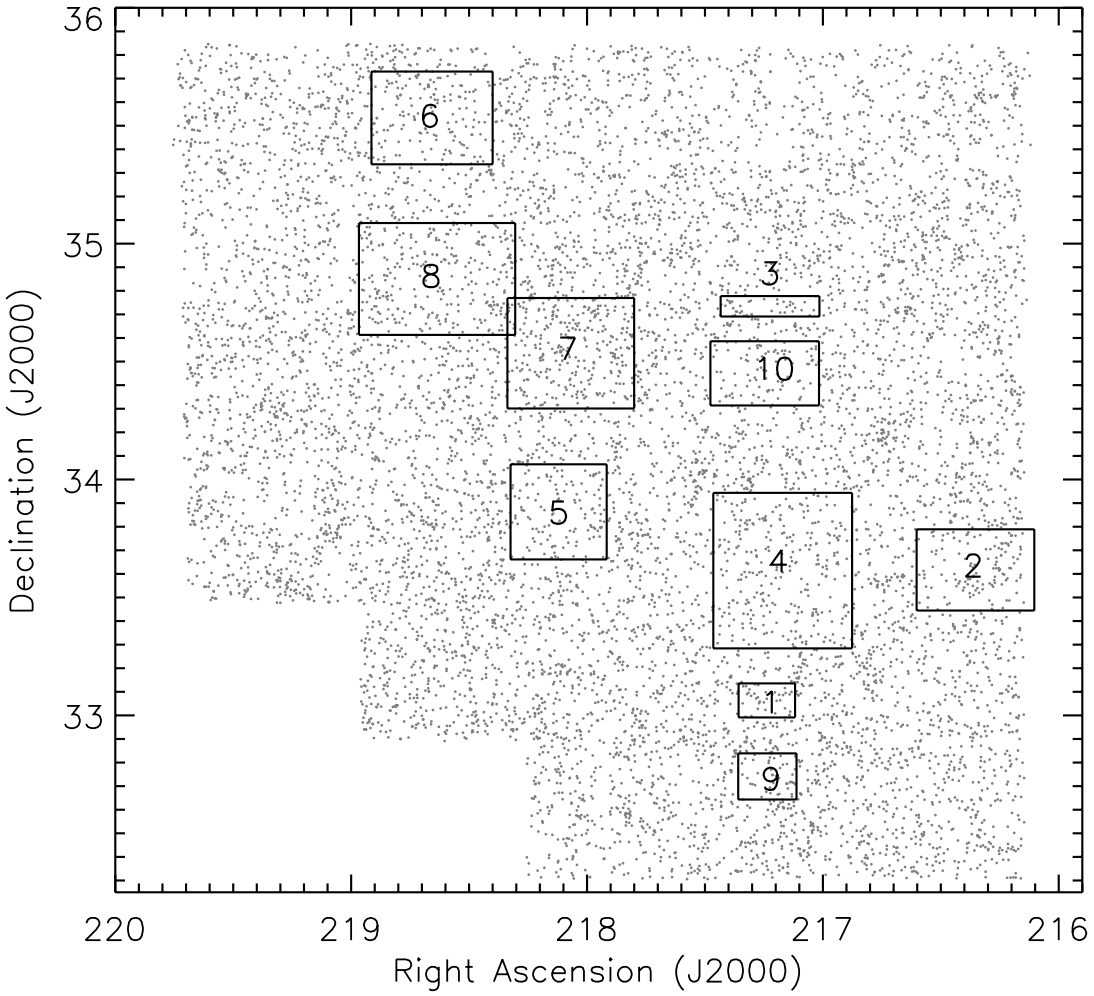

FIG. 3.—Map of the NDWFS survey area with the coverage of the co-added *z*Bootes fields overlayed. As in Fig. 1, the gray points show the distribution of 25% of the $I < 21.5$ extended sources from the NDWFS catalogs. The number marking each of the co-added subfields denotes the field number assigned to that subfield. The co-added imaging covers 1.24 deg^2 of the 7.62 deg^2 *z*Bootes region.

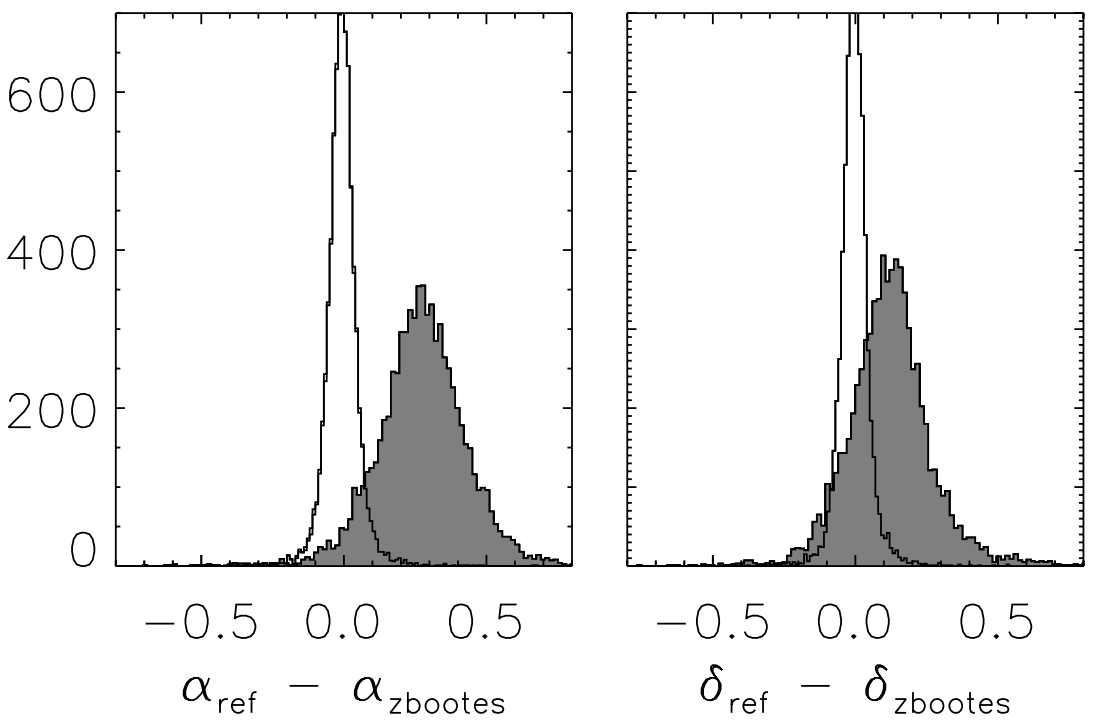

FIG. 4.—Histogram of astrometric offsets (in arcsec) between sources reported by *z*Bootes and SDSS (*open histogram*) and *z*Bootes and NDWFS (*filled histogram*). Only well-detected stars are used in this plot, so photon noise is not the dominant source of uncertainty in the astrometry. In general, SDSS and *z*Bootes agree quite well (50 mas rms). There are offsets between the *z*Bootes and NDWFS for each of the subfields, resulting in a overall mean offset and larger dispersion seen in the comparison between the *z*Bootes and NDWFS coordinates.

TABLE 1
Astrometric Offsets between zBootes and NDWFS

Field Name	$\Delta\alpha$ (arcsec)	$\Delta\delta$ (arcsec)
b1-1	−0.37	−0.31
b1-2	−0.30	−0.37
b1-3	−0.22	−0.18
b1-4	−0.29	−0.15
b2-1	−0.30	−0.05
b2-2	−0.22	−0.04
b2-3	−0.24	−0.08
b2-4	−0.21	−0.09
b3-1	−0.20	−0.13
b3-2	−0.23	−0.10
b3-3	−0.25	−0.15
b3-4	−0.27	−0.13
b4-1	−0.03	−0.05
b4-2	−0.01	0.01
b4-3	−0.11	−0.10
b4-4	−0.11	−0.11
b5-1	−0.17	0.02
b5-2	−0.30	−0.12
b5-3	−0.20	0.08
b5-4	−0.28	−0.18
b6-1	−0.32	−0.13
b6-2	−0.25	−0.17
b6-3	−0.31	−0.12
b6-4	−0.24	−0.09
b7-1	−0.22	−0.12
b7-2	−0.26	−0.10
b7-3	−0.28	−0.11
b7-4	−0.30	−0.13
b8-1	−0.35	−0.10
b8-2	−0.37	−0.17
b8-3	−0.26	−0.04
b8-4	−0.33	−0.12
mos-01	−0.17	−0.10
mos-02	−0.25	−0.22
mos-03	−0.21	−0.10
mos-04	−0.20	−0.17
mos-05	−0.33	−0.11
mos-06	−0.21	0.07
mos-07	−0.30	−0.12
mos-08	−0.32	−0.00
mos-09	−0.13	0.04
mos-10	−0.21	−0.07

zBootes and SDSS coordinates is ∼50 milliarcsec (mas) per coordinate, while the agreement with NDWFS is poorer with a dispersion of nearly 130 mas per coordinate. SDSS astrometry has a 45 mas dispersion per coordinate (Pier et al. 2003), so the zBootes astrometric error is dominated by astrometric errors in the SDSS catalogs. Also, notice that the NDWFS and zBootes astrometric have systematic offsets in both directions, likely due to the different astrometric reference systems used by NDWFS and SDSS imaging. Robust comparisons between NDWFS and zBootes (or SDSS) thus require the removal of these offsets to properly match objects in each catalog. Table 1 lists the average shifts between the astrometry of each zBootes field and the NDWFS catalog.

4.4. *Survey Depth*

The depth of the zBootes images varies between each field and as a function of position in each field itself due to the variable number of exposures taken for each field and variable conditions during the observations. In order to quantify the depth of our catalogs near each detected object, we added fake point sources with the same point spread function as measured from nearby unsaturated stars in the zBootes images. For each field, we perform 10 simulations with each simulation consisting of 3000 fake stars added to the co-added frame of each field. We then record the average 50% completeness in a 10′ diameter region around each object detected in our catalogs. Figure 5 illustrates the variations in the survey depth within a single zBootes field. As illustrated in the figure, the variations in survey depth can be as large as 0.5 mags across the field.

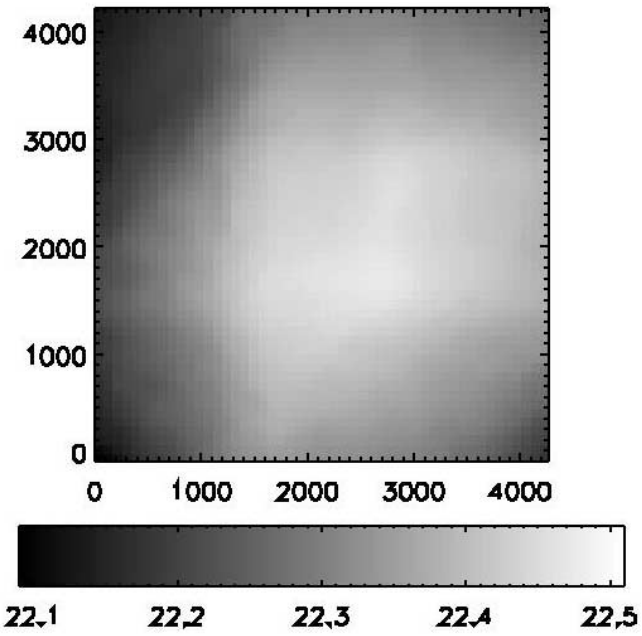

Fig. 5.—Map of the 50% completeness limit of the b4-1 field in pixel coordinates. The depth of the catalogs are a strong function of position in the final mosaicked image. This is primarily due to the decreased number of exposures that were co-added near the edge of the mosaicked field. The completeness can vary as much as 0.5 mag from the center of the field to the edge.

Figure 6 shows the fraction of the zBootes coverage area as a function of the 50% completeness depth and as a function of the 3 σ detection limits of the catalogs. The final zBootes catalog is 50% complete to 22.4 mag over 90% of the survey area and 50% of the survey area is complete to 22.7 mag. Thus, the zBootes catalogs reach more than 2 mag fainter than SDSS over the entire survey region. The mosaicked images of the overlapping zBootes fields reach fainter limits than the single frames. Of the 1.24 deg^2 covered in the overlapping fields, 50% of the area is complete to 23.3 mag and 90% is complete to 23.1 mag. Table 2 lists the average 50% completeness limit of each of the zBootes subfields. The zBootes data are thus sensitive to L^* galaxies to $z \sim 1$ and should provide extra constraint on photometric redshifts measurements for galaxies at $0 < z < 1$.

5. DATA PRODUCTS

5.1. *Images*

Images and weight maps [`fieldname.fits, fieldname-weight.fits`].—We release the final co-added images and the associated weight map for each. The images are in ADU counts per pixel and the magnitude zero point of the photometry of each image is stored in the `MAGZERO` header keyword. The weight maps are normalized such that each pixel reflects the number of exposures that contributed to the image. All of these images have

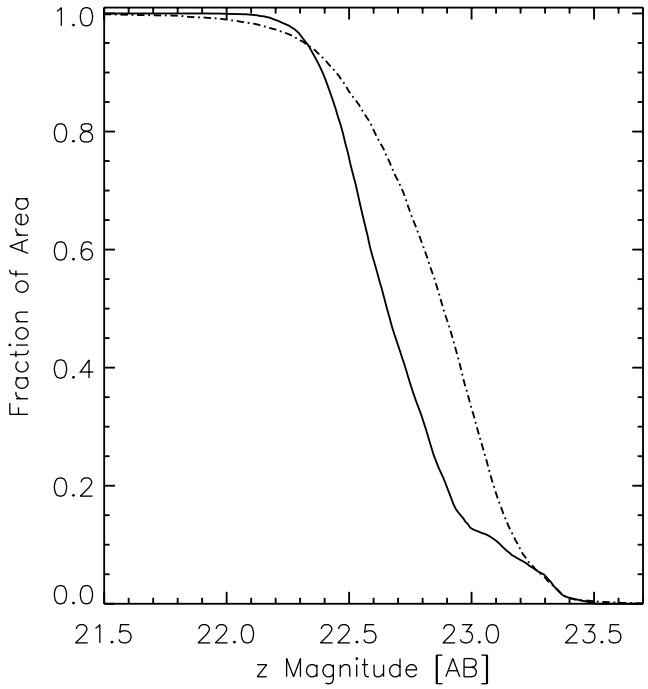

FIG. 6.—Fraction of the *z*Bootes survey area as function of the 50% completeness limit and 3 σ detection limit of the *z*Bootes catalogs. The solid line shows the fraction of the *z*Bootes 7.6 deg^2 area as a function of the 50% completeness, while the dot-dashed line shows the fraction of the survey area versus the 3 σ detection limit in a 3″ aperture. The *z*Bootes catalog is complete to 22.4 mag over 90% of the survey area and 50% of the area is complete to 22.7 mag or deeper. The knee in the distribution of 50% completeness limit near $z = 23.0$ is due the deeper limits present in the co-added *z*Bootes fields as discussed in the text.

world-coordinate system information in the headers. Note that the orientation of these images corresponds to the orientation of the 90Prime images on the sky (north is to the right and east is upward) and not the standard image orientation.

Regions of the sky that were observed in multiple *z*Bootes fields were co-added as described in § 3. The resulting images are flux calibrated and have units of nanomaggies per pixel. A nanomaggie is a flux-density unit equal to 10^{-9} of a magnitude zero source. Since we calibrated the *z*Bootes photometry to SDSS, and SDSS is nearly an AB system, 1 nanomaggie corresponds to 3.631 μJy or 3.631×10^{-29} erg s^{-1} cm^{-2} Hz^{-1}. As above, the weight maps associated with each of the mosaic images reports the total number of 300 s exposures that contributed to each pixel.

Photometric catalogs [`fieldname-cat.fits`].—We also release binary FITS files of the SExtractor catalog for each *z*Bootes field as well as overlapping regions. In each file, we report the measured properties of each of the objects detected in the *z*Bootes imaging. A majority of the parameters listed in the catalogs are standard SExtractor outputs, so we will not repeat the definitions. The aperture fluxes and magnitudes reported in the *z*Bootes catalogs are measured at 12 diameters. The diameters run from 1″ to 10″ in steps of 1″; the final two apertures have diameters of 15″ and 20″. The nonstandard parameters included in each of the catalogs are as follows.

1. `NOBS` [integer].—Mean number of observations (300 s exposures) that contribute to the pixels each object falls on. Objects with less than *NOBS* $\lesssim 5$ should be used with caution.

2. `ERR_[1,3,5,7]` [float].—Photometric error in a [1, 3, 5, 7] arcsec diameter aperture determined from the dispersion in the local sky background within a 6′ radius around each object.

TABLE 2
AVERAGE COMPLETENESS LIMITS (50%) OF *z*BOOTES FIELDS

Field Name	Depth (mag)
b1-1	22.35
b1-2	22.50
b1-3	22.54
b1-4	22.52
b2-1	22.59
b2-2	22.68
b2-3	22.79
b2-4	22.72
b3-1	22.56
b3-2	22.69
b3-3	22.67
b3-4	22.63
b4-1	22.58
b4-2	22.50
b4-3	22.76
b4-4	22.63
b5-1	22.39
b5-2	22.48
b5-3	22.46
b5-4	22.41
b6-1	22.85
b6-2	22.93
b6-3	22.95
b6-4	22.88
b7-1	22.81
b7-2	22.91
b7-3	22.95
b7-4	22.80
b8-1	22.63
b8-2	22.68
b8-3	22.73
b8-4	22.69
mos-01	22.87
mos-02	23.13
mos-03	23.05
mos-04	23.25
mos-05	23.17
mos-06	23.35
mos-07	23.33
mos-08	23.38
mos-09	22.84
mos-10	23.33

NOTE.—Depth is estimated by the 50% completeness limit of the catalogs.

3. `COMP50` [float].—The 50% completeness limit determined by inserting ~30,000 fake point sources into the images and measuring the fraction recovered using the same analysis procedure as that used when constructing the catalogs. The local completeness is calculated within a 10′ region around each object.

4. `DETECT_3SIG_3ARC` [float].—The local 3 σ detection limit determined in a 3″ diameter aperture around each object based on measurements of the local variation in the sky background.

5. `PHOTFLAG` [integer].—For each object, this flag is set if any of the pixels contributing to the object detection were in the nonlinear or saturated regime on the 90Prime CCDs. Photometry for objects with this flag set should be used with caution.

Final merged catalog [`zbootes-cat.fits`].—The final catalog represents the merged catalog for the *z*Bootes imaging. For

objects included in multiple individual catalogs, the observation with the smallest photometric error is declared the primary observation and included in the final catalog. Objects in the final catalog were cross-matched to the NDWFS optical catalogs using a 1″ search radius. Before the cross-matching was performed, the locally determined astrometric offsets between the *z*Bootes and NDWFS astrometric systems (reported in Table 1) were removed. The following parameters are included in the final catalog but are not in the individual catalogs.

1. `FIELDNAME` [string].—Name of the *z*Bootes field in which the photometric quantities for each object were measured.

2. `DUPLICATE` [integer].—Flag that is set if a given object was detected in multiple catalogs. If an object was detected in multiple frames, then the observation with the lowest photometric error was declared to be the best and included in the final merged catalog; each object is listed in the final catalog only once.

3. `NDWFS_NAME` [string].—Name of the nearest NDWFS object to each *z*Bootes detection. The catalogs were compared with a 1″ search radius; if there were no NDWFS objects within the search radius of the *z*Bootes object, this entry is empty.

4. `NDWFS_RA` [double].—Right ascension of the nearest NDWFS object to the *z*Bootes detection in decimal degrees.

5. `NDWFS_DEC` [double].—Declination of the nearest NDWFS object to the *z*Bootes detection in decimal degrees.

6. CATALOG AVAILABILITY

The *z*Bootes catalogs described in this paper are available for download online.[3] Any use of these data should include references to this paper. If any of the cross-identifications to the NDWFS catalogs are used, the appropriate citations should be made to the papers describing those data.

R. J. C. was funded through a National Science Foundation Graduate Research Fellowship. We are grateful to Ed Olszewski, Grant Williams, and Mike Lessar for providing the 90Prime instrument and technical information critical to the reduction and calibration of this data set. We thank Buell Jannuzi and Arjun Dey and the NOAO technical staff for hosting the data provided by this release. Daniel Eisenstein, Michael Brown, and Jane Rigby provided many useful comments and suggestions during the reduction and calibration of this data set.

Facilities: Bok (90Prime)

[3] See http://archive.noao.edu/nsa/zbootes.html.

REFERENCES

Adelman-McCarthy, J. K., et al. 2006, ApJS, 162, 38
Becker, R. H., White, R. L., & Helfand, D. J. 1995, ApJ, 450, 559
Bertin, E., &Arnouts, S. 1996, A&AS, 117, 393
Brand, K., et al. 2005, ApJ, 626, 723
———. 2006a, ApJ, 641, 140
———. 2006b, ApJ, 644, 143
Brown, M. J. I., Dey, A., Jannuzi, B. T., Lauer, T. R., Tiede, G. P., & Mikles, V. J. 2003, ApJ, 597, 225
Brown, M. J. I., Jannuzi, B. T., Dey, A., & Tiede, G. P. 2005, ApJ, 621, 41
Brown, M. J. I., et al. 2006, ApJ, 638, 88
Cool, R. J., et al. 2006, AJ, 132, 823
Dawson, S., et al. 2004, ApJ, 617, 707
Desai, V., et al. 2006, ApJ, 641, 133
de Vries, W. H., Morganti, R., Röttgering, H. J. A., Vermeulen, R., van Breugel, W., Rengelink, R., & Jarvis, M. J. 2002, AJ, 123, 1784
Dey, A., et al. 2005, ApJ, 629, 654
Eisenhardt, P. R., et al. 2004, ApJS, 154, 48
Elston, R. J., et al. 2005, ApJ, 639, 816
Higdon, J. L., et al. 2005, ApJ, 626, 58
Ivezić, Ž., et al. 2004, Astron. Nachr., 325, 583
Kenter, A., et al. 2005, ApJS, 161, 9
Khan, S. A., et al. 2005, ApJ, 631, L9
Kollmeier, J. A., et al. 2006, ApJ, 648, 128
Murray, S. S., et al. 2005, ApJS, 161, 1
Oke, J. B. 1974, ApJS, 27, 21
Pier, J. R., Munn, J. A., Hindsley, R. B., Hennessy, G. S., Kent, S. M., Lupton, R. H., & Ivezić, Ž. 2003, AJ, 125, 1559
Rhoads, J. E., Malhotra, S., Dey, A., Stern, D., Spinrad, H., & Jannuzi, B. T. 2000, ApJ, 545, L85
Rhoads, J. E., et al. 2003, AJ, 125, 1006
———. 2004, ApJ, 611, 59
Stanford, S. A., et al. 2005, ApJ, 634, L129
Stern, D., et al. 2005, ApJ, 631, 163
———. 2006, ApJ, submitted (astro-ph/0608603)
Wang, J. X., et al. 2004, ApJ, 608, L21
Weedman, D. W., et al. 2006, ApJ, 651, 101
Williams, G. G.,Olszewski, E., Lesser, M. P., & Burge, J. H. 2004, Proc. SPIE, 5492, 787